Fourier modal method for the description of nanoparticle lattices in the dipole approximation

Ilia M. Fradkin,[1,2,*] Sergey A. Dyakov,[1] and Nikolay A. Gippius[1]
[1]*Skolkovo Institute of Science and Technology, Nobel Street 3, Moscow 143025, Russia*
[2]*Moscow Institute of Physics and Technology, Institutskiy pereulok 9, Moscow Region 141701, Russia*

(Received 29 December 2018; revised manuscript received 13 February 2019; published 27 February 2019)

Rigorous coupled-wave analysis (RCWA) is a very effective tool for studying optical properties of multilayered vertically invariant periodic structures. However, it fails to deal with arrays of small particles because of high gradients in a local field. In this paper, we implement the discrete dipole approximation (DDA) for the construction of scattering matrices of arrays of resonant nanoparticles. This strongly speeds up the calculations and therefore provides an opportunity for thorough consideration of various layered structures with small periodic inclusions in terms of the RCWA. We demonstrate the performance of the proposed method by considering plasmonic lattices embedded in a homogeneous ambience and placed inside and onto an optical waveguide. Both localized surface plasmon resonances (LSPRs) and lattice plasmon resonances (LPRs) are observed as well as their hybridization with photonic guided modes. High accuracy and fast convergence of our approach are shown by comparison with the finite element method (FEM) and RCWA calculations correspondingly.

DOI: 10.1103/PhysRevB.99.075310

I. INTRODUCTION

Periodic photonic structures are one of the most important low-level components in modern photonics since they form the basis for plenty of optical elements and devices. They include band-gap materials [1–3], diffraction gratings [4–7], frequency selective surfaces [8], antennas [9,10], waveguides [11–13], metasurfaces [14–18], biosensors, etc. Spatial periodicity naturally suggests that the electromagnetic field in periodic structures can be expanded into the Fourier series, which appears to be an effective tool for calculating of optical properties of such structures. Indeed, this is a basic idea of the rigorous coupled-wave analysis (RCWA) [13,19] proved itself to be an extremely fast and efficient computational method. However, inclusions much smaller than a wavelength give rise to high gradients in the near field, which forces to take lots of harmonics into account and can significantly slow down this approach. This fundamental drawback of all Fourier-modal methods, which originates from the Gibbs phenomenon [20,21], is most pronounced for high-contrast inclusions, such as plasmonic nanoparticles. Moreover, occurring of localized surface plasmon resonances makes the contribution of these inclusions determinative for the optical properties of the whole structure.

To overcome this problem, several approaches have been developed. One of them is the Li factorization rules [22], which solve the problem of poor convergence at concurrent jump discontinuities. Yet another approach is the use of an adaptive spatial resolution by choosing specially designed coordinate transformation which increases the resolution around the material boundaries [23,24]. These methods significantly improve the convergence of the RCWA numerical scheme. However, if the size of metal inclusions is much smaller than the structure spatial period, practically unrealizable number of Fourier harmonics is required for the solution of Maxwell's equations to be converged. As a result, the RCWA fails to describe optical properties of a periodic array of metallic particles in a dielectric. At the same time, the light scattering by relatively small particles in most cases might be approximately described by substituting them with ideal electric dipoles, which brings us to discrete dipole approximation [25] (DDA).

In this paper, we report the approach for calculation of a scattering matrix of a plasmonic lattice, which is based on a determination of an effective polarizability tensor of nanoparticles arranged in periodic arrays. We combine three widespread numerical methods: finite element method (FEM), DDA, and RCWA in order to implement each of them on a specific stage of computation and obtain precise results in a fast way. It helps to study any layered structures with inclusions of plasmonic lattices for any angles of incident light. Such an approach makes it possible to observe dispersion of lattice waves and phenomena of out-of-plane polarization of plasmonic particles [26,27]. To illustrate the feasibility of the proposed method, we consider the same plasmonic lattice in a homogeneous ambience, on a photonic waveguide and inside it, the formation of photonic band structure, strong coupling of photonic guided modes with both LSPRs and LPRs. To verify our approach, we compare the obtained results with calculations conducted by conventional RCWA and FEM.

II. EFFECTIVE POLARIZABILITY

Dipole approximation makes it possible to split the problem of determination of particle polarization into two parts, which deal with a problem in different scales. Indeed, when a

*ilia.fradkin@skoltech.ru

particle is incorporated in a certain structure of permittivity $\varepsilon^{\text{bg}}(\mathbf{r})$ so that this permittivity is constant over the volume of a particle then it can be conveniently substituted with a solitary dipole (see Appendix A). The dipole moment of the ith particle $\mathbf{P}_i$ is determined as a polarizability tensor $\hat{\alpha}$, acting on a background low-gradient electric field $\mathbf{E}_i^{\text{bg}}$, which excites electron oscillations in a plasmonic nanoparticle:

$$\mathbf{P}_i = \hat{\alpha}\mathbf{E}_i^{\text{bg}}. \tag{1}$$

In this paper, we define dipole moment $\mathbf{P}_i$ as a dipole moment of free charges, which generates the same far field as a real particle. To give an example, such a definition makes $\hat{\alpha}$ tensor ε^{bg} times larger in comparison with a tensor conventionally defined for a particle in a homogeneous medium [28]. Computation of this polarizability tensor is the first subproblem, which can be easily solved numerically by any near-field computational method for a particle of any shape (see Appendix A) or even analytically for particles of trivial shape [29,30]. The second subproblem is a determination of the background field itself $\mathbf{E}_i^{\text{bg}}$, which is a sum of an incident wave field $\mathbf{E}_i^0$, which would have been in the absence of the lattice and electric field scattered by all the neighboring particles of a lattice at the coordinate of the considered particle, $\mathbf{r}_i$:

$$\mathbf{E}_i^{\text{bg}} = \mathbf{E}_i^0 + \sum_{j\neq i} \hat{G}(\mathbf{r}_i, \mathbf{r}_j)\mathbf{P}_j, \tag{2}$$

where $\hat{G}(\mathbf{r}_i, \mathbf{r}_j)$ is the dyadic Green's function showing electric field induced at the point $\mathbf{r}_i$ by a dipole at the coordinate $\mathbf{r}_j$ in a considered, not necessarily homogeneous environment. It should be emphasized that in this expression Green's function acts on a dipole moment of free charges and is defined accordingly.

Background electric field can be found immediately by solving this linear algebraic system consisting of $3N$ equations (N is a number of particles) via any specialized method [31], which is a general approach for DDA method. However, when an infinite lattice is considered (see Fig. 1), then according to Bloch theorem the Floquet periodicity occur, which helps to solve the system analytically [31–38]:

$$\mathbf{E}_i^{\text{bg}} = (\hat{I} - \hat{C}(\mathbf{k}_\parallel)\hat{\alpha})^{-1}\mathbf{E}_i^0, \tag{3}$$

where $\hat{I}$ is the identity matrix, $\mathbf{k}_\parallel$ is the in-plain component of photon wave vector, and $\hat{C}$ tensor is a so-called dynamic interaction constant [37], which is a sum of dyadic Green's function over the lattice (see Appendix B for details of practical calculation):

$$\hat{C}(\mathbf{k}_\parallel) = \sum_{j\neq i} \hat{G}(\mathbf{r}_i, \mathbf{r}_j)e^{-i\mathbf{k}_\parallel(\mathbf{r}_i-\mathbf{r}_j)}. \tag{4}$$

Relation (3) allows to introduce effective polarizability tensor $\hat{\alpha}^{\text{eff}}$, which connects dipole moment with an incident electric field $\mathbf{P}_i = \hat{\alpha}^{\text{eff}}\mathbf{E}_i^0$:

$$\hat{\alpha}^{\text{eff}} = \hat{\alpha}(\hat{I} - \hat{C}(\mathbf{k}_\parallel)\hat{\alpha})^{-1}. \tag{5}$$

As it can be seen from this expression, effective polarizability $\hat{\alpha}^{\text{eff}}$ has resonances of two types. The first one occurs, when the ordinary individual polarizability $\hat{\alpha}$ experiences wide LSPR. Another resonance with nontrivial dispersion (LPR) is associated with collective oscillations of the lattice and occurs when the condition $\hat{C}(\mathbf{k}_\parallel) = \hat{\alpha}^{-1}$ is fulfilled.

This approach allows to describe the structure in a very simple way but naturally has inherent limitations. Indeed, dipole approximation works until background field does not change on the dimensions of a particle, which results in a requirement for a particle to be much less than a wavelength (far-field limit) and a period of a structure (near-field limit). Also, an electric field of an ideal dipole and a real particle match each other for distances larger than several particle sizes. This means that all the in the vicinity of particles should be accounted in $\hat{\alpha}^{\text{eff}}$ tensor by an appropriate choice of Green's function and polarizability of a single particle $\hat{\alpha}$.

Dipole approximation allows considering a wide range of structures. However, the proposed approach can be naturally extended by taking into account higher-order multipole moments. Even accounting for quadrupole moment makes it possible to consider larger particles, place them closer to each other and observe quadrupole resonances. For instance, this can be potentially profitable for the description of dense plasmonic metasurfaces or periodic structures of large dielectric particles.

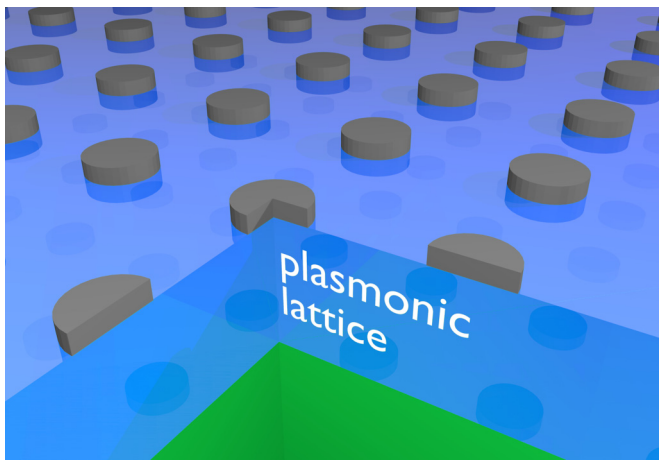

FIG. 1. Sketch of a plasmonic lattice embedded in a homogeneous layer of a typical layered structure.

III. SCATTERING MATRIX CALCULATION

Calculation of the effective polarizability $\hat{\alpha}^{\text{eff}}$ of a particle in a lattice is an important stage. However, our final goal is to obtain the total scattering matrix of the entire structure containing resonant particles. For this hereafter, we will use the formalism of RCWA which was conveniently developed for calculating of optical properties of vertically invariant periodic structures (e.g., multilayered gratings). The total scattering matrix of a multilayered structure is calculated iteratively [39]; at each iteration step, the scattering matrix of the ith layer is connected with the total scattering matrix of layers 1 to $i-1$ found at previous iteration step. Usually, the scattering matrix of each layer is found by decomposing the electromagnetic field into spatial Fourier harmonics.

As mentioned above, such structures as small metallic particles cause high-gradient fields, which requires taking

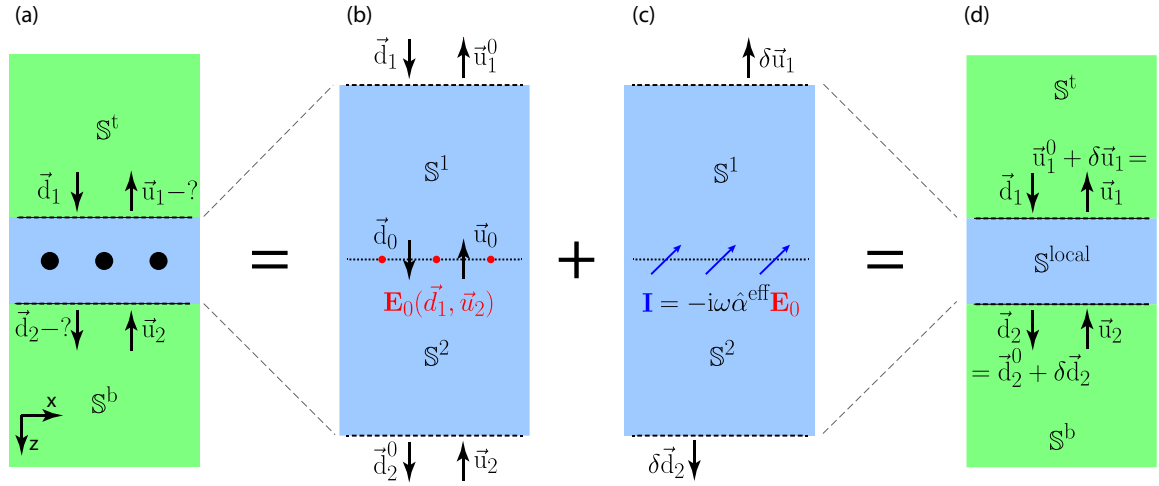

FIG. 2. Calculation of the scattering matrix of a plasmonic lattice in dipole approximation. (a) Nanoparticles lattice in a layered medium. (b) Calculation of external field at the position of nanoparticles (red points) in the layered medium without nanoparticles. (c) Calculation of current densities (blue arrows) at the position of nanoparticles. (d) Calculation of the local scattering matrix. In (a)–(d), dashed lines separate the local dielectric environment of the nanoparticles (blue color) from the outer dielectric environment (green color). Both local and outer dielectric environments might include any number of vertically homogeneous layers and interfaces between them.

into account a very large number of spatial harmonics to resolve them in RCWA. However, strongly evanescent behavior of high-$\mathbf{k}_\parallel$ harmonics leads to their confinement inside a layer of several dozens nanometers thickness, which contains plasmonic nanoparticles (blue region in Fig. 2). This means that construction of the scattering matrix of this layer as a whole, $\mathbb{S}^{\text{local}}$, via DDA gives us a possibility to work only with low-$\mathbf{k}_\parallel$ harmonics [see Fig. 2(a)]. In such an approach, all high-$\mathbf{k}_\parallel$ effects are described by the effective $\hat{\alpha}^{\text{eff}}$, while low-$\mathbf{k}_\parallel$ effects are treated conventionally by RCWA. Once the local scattering matrix $\mathbb{S}^{\text{local}}$ is calculated, the initial RCWA problem of calculation of the total scattering matrix takes on the task of coordination of adjacent layers, which is consistent with the original spirit of RCWA.

By definition, the scattering matrix of the considered layer, $\mathbb{S}^{\text{local}}$, connects amplitudes of the incoming and outgoing waves on the boundaries of the considered layer [see Fig. 2(a)] [13]:

$$\begin{bmatrix} \vec{d}_2 \\ \vec{u}_1 \end{bmatrix} = \mathbb{S}^{\text{local}} \begin{bmatrix} \vec{d}_1 \\ \vec{u}_2 \end{bmatrix}. \tag{6}$$

Hereinafter, we use the symbols $\vec{d}$ and $\vec{u}$ for the amplitudes of positively and negatively propagating waves taken at positions specified by the subscripts as shown in Fig. 2. Please note that z axis is directed from top to bottom.

Elaborating the idea discussed in the section II we represent this matrix as a sum of two terms $\mathbb{S}^{\text{local}} = \mathbb{S}_0^{\text{local}} + \delta\mathbb{S}^{\text{local}}$. The first term corresponds to a matrix calculated in the assumption of the absence of a lattice inclusion [see Fig. 2(b)], whereas the second one [see Fig. 2(c)] accounts for the radiation of the currents induced in the particles. Finally, we substitute the complex layer that contains nanoparticles lattice by a black box, which is fully described by the matrix $\mathbb{S}^{\text{local}}$, which has a small number of nonzero elements, describing low-$\mathbf{k}_\parallel$ harmonics.

We start with the consideration of an empty layer without plasmonic inclusions. Scattering matrix $\mathbb{S}_0^{\text{local}}$ connects amplitudes on the boundaries:

$$\begin{bmatrix} \vec{d}_2^0 \\ \vec{u}_1^0 \end{bmatrix} = \mathbb{S}_0^{\text{local}} \begin{bmatrix} \vec{d}_1 \\ \vec{u}_2 \end{bmatrix}. \tag{7}$$

However, for our purposes, it is very important to know the vector of amplitudes $[\vec{d}_0, \vec{u}_0]^T$ at the plane, which will further contain the dipole lattice. Therefore we introduce scattering matrices $\mathbb{S}^1$ and $\mathbb{S}^2$ of upper and lower parts of the layer, respectively. These matrices act as follows:

$$\begin{bmatrix} \vec{d}_0 \\ \vec{u}_1^0 \end{bmatrix} = \mathbb{S}^1 \begin{bmatrix} \vec{d}_1 \\ \vec{u}_0 \end{bmatrix}, \quad \begin{bmatrix} \vec{d}_2^0 \\ \vec{u}_0 \end{bmatrix} = \mathbb{S}^2 \begin{bmatrix} \vec{d}_0 \\ \vec{u}_2 \end{bmatrix}, \tag{8}$$

Moreover, they are obviously connected as

$$\mathbb{S}_0^{\text{local}} = \mathbb{S}^1 \otimes \mathbb{S}^2, \tag{9}$$

where the operand $\otimes$ denotes the combination of two adjacent scattering matrices [39] (see Appendix C for details of its calculations).

It is convenient to introduce an auxiliary matrix $\mathbb{B}^{\text{in}}$, which allows to determine $[\vec{d}_0, \vec{u}_0]^T$ vectors directly from the incoming waves amplitudes. Equations (8) allows us to represent this matrix via $\mathbb{S}^1$ and $\mathbb{S}^2$ components:

$$\begin{bmatrix} \vec{d}_0 \\ \vec{u}_0 \end{bmatrix} = \mathbb{B}^{\text{in}} \begin{bmatrix} \vec{d}_1 \\ \vec{u}_2 \end{bmatrix}, \quad \mathbb{B}^{\text{in}} = \begin{bmatrix} \mathbb{D}_1\mathbb{S}_{11}^1 & \mathbb{D}_1\mathbb{S}_{12}^1\mathbb{S}_{22}^2 \\ \mathbb{D}_2\mathbb{S}_{21}^2\mathbb{S}_{11}^1 & \mathbb{D}_2\mathbb{S}_{22}^2, \end{bmatrix}, \tag{10}$$

where

$$\mathbb{D}_1 = \left(1 - \mathbb{S}_{12}^1\mathbb{S}_{21}^2\right)^{-1}, \tag{11}$$

$$\mathbb{D}_2 = \left(1 - \mathbb{S}_{21}^2\mathbb{S}_{12}^1\right)^{-1}. \tag{12}$$

Vector $[\vec{d}_0, \vec{u}_0]^T$ help us to determine subsequently the field, $\mathbf{E}^0$, induced at the position of the particle and cor-

responding current $\mathbf{I} = -i\omega\hat{\alpha}^{\text{eff}}\mathbf{E}^0$. According to Maxwell's equations, the presence of currents leads to an appearance of discontinuities of the horizontal components of electric and magnetic fields [40,41]. As a result, the vectors of amplitudes taken at the coordinates infinitesimally above and below the dipole plane [see Fig. 2(c)] are connected as follows:

$$\begin{bmatrix}\vec{\mathrm{d}}\\ \vec{\mathrm{u}}\end{bmatrix}_{z_p+0} - \begin{bmatrix}\vec{\mathrm{d}}\\ \vec{\mathrm{u}}\end{bmatrix}_{z_p-0} = \begin{bmatrix}\vec{\mathrm{j}}_d\\ \vec{\mathrm{j}}_u\end{bmatrix} = \mathbb{A}[\hat{\alpha}^{\text{eff}}]\begin{bmatrix}\vec{\mathrm{d}}_0\\ \vec{\mathrm{u}}_0\end{bmatrix}, \tag{13}$$

where $[\vec{\mathrm{j}}_d, \vec{\mathrm{j}}_u]^T$ is the amplitude discontinuity vector determined by the induced current $\mathbf{I}$, which results in a connection with incoming wave amplitudes via a special tensor $\mathbb{A}[\hat{\alpha}^{\text{eff}}]$, (see Appendix C).

The last thing, which is left to do is the calculation of outgoing from the layer wave amplitudes, determined by this emission. Similarly to $\mathbb{B}^{\text{in}}$, it is very convenient to introduce another matrix $\mathbb{B}^{\text{out}}$ connecting these discontinuities with outgoing wave amplitudes associated with them. This matrix can be expressed through scattering matrices $\mathbb{S}^1$ and $\mathbb{S}^2$ components from the condition of the absence of incoming waves [see Fig. 2(c)]:

$$\begin{bmatrix}\delta\vec{\mathrm{d}}_2\\ \delta\vec{\mathrm{u}}_1\end{bmatrix} = \mathbb{B}^{\text{out}}\begin{bmatrix}\vec{\mathrm{j}}_d\\ \vec{\mathrm{j}}_u\end{bmatrix}, \quad \mathbb{B}^{\text{out}} = \begin{bmatrix}\mathbb{S}^2_{11}\mathbb{D}_1 & -\mathbb{S}^2_{11}\mathbb{D}_1\mathbb{S}^1_{12}\\ \mathbb{S}^1_{22}\mathbb{D}_2\mathbb{S}^2_{21} & -\mathbb{S}^1_{22}\mathbb{D}_2\end{bmatrix}. \tag{14}$$

It should be especially emphasized, that although there are no incoming waves in the subproblem of dipole radiation, their amplitudes depend on the incoming waves, which allows finding the correction to the scattering matrix $\delta\mathbb{S}^{\text{local}}$ defined as

$$\begin{bmatrix}\delta\vec{\mathrm{d}}_2\\ \delta\vec{\mathrm{u}}_1\end{bmatrix} = \delta\mathbb{S}^{\text{local}}\begin{bmatrix}\vec{\mathrm{d}}_1\\ \vec{\mathrm{u}}_2\end{bmatrix}. \tag{15}$$

Summing up, in order to do this, we just have to (I) calculate the incoming wave amplitudes at a plane of the particles, (II) apply $\mathbb{A}[\hat{\alpha}^{\text{eff}}]$ operator in order to find the amplitude discontinuity vector $[\vec{\mathrm{j}}_d, \vec{\mathrm{j}}_u]^T$ and finally (III) determine the correction to the outgoing from the layer waves.

Combining Eqs. (10)–(15), we obtain the following expression for the correction to the scattering matrix of the layer:

$$\delta\mathbb{S}^{\text{local}} = \mathbb{B}^{\text{out}}\mathbb{A}\mathbb{B}^{\text{in}}. \tag{16}$$

When the local scattering matrix of a plasmonic layer is known, it can be easily inserted in any structure. Its total scattering matrix is then found as

$$\mathbb{S}^{\text{tot}} = \mathbb{S}^t \otimes \mathbb{S}^{\text{local}} \otimes \mathbb{S}^b. \tag{17}$$

These rather general expressions can be potentially used for a description of rather complex structures, for example, a plasmonic lattice inside a photonic crystal or a lattice on a metamaterial. However, in this paper, we implement our approach only for two most practical cases and it makes sense to specify $\mathbb{B}$ matrices for them. When the lattice is embedded in a homogeneous medium, $\mathbb{B}$ matrices take a very simple

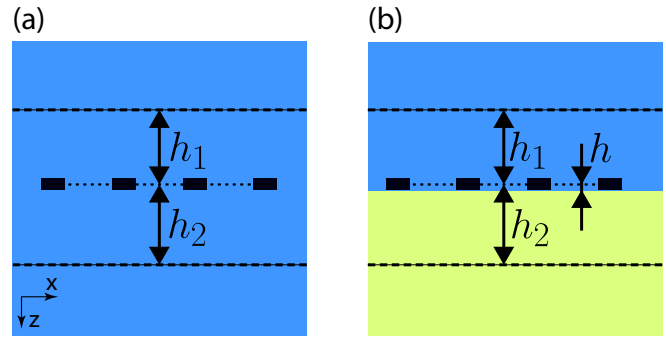

FIG. 3. Sketch of the two most practical structures: (a) nanoparticles in homogeneous medium and (b) nanoparticles on an interface. Dashed lines bound the local dielectric environment of the nanoparticles. Dotted lines connects the nanoparticles centers.

form:

$$\mathbb{B}^{\text{in}} = \begin{bmatrix}e^{ik_0\hat{K}_z h_1} & \hat{0}\\ \hat{0} & e^{ik_0\hat{K}_z h_2}\end{bmatrix}, \quad \mathbb{B}^{\text{out}} = \begin{bmatrix}e^{ik_0\hat{K}_z h_2} & \hat{0}\\ \hat{0} & -e^{ik_0\hat{K}_z h_1}\end{bmatrix}, \tag{18}$$

where h_1 and h_2 are the thicknesses of higher and lower layers included into the local environment (see Fig. 3) and $\hat{K}_z$ satisfies the relation

$$\hat{K}_x^2 + \hat{K}_y^2 + \hat{K}_z^2 = \varepsilon\hat{I}. \tag{19}$$

In Eqs. (18) and (19), $\hat{K}_x$, $\hat{K}_y$, and $\hat{K}_z$ are the dimensionless diagonal operators [13] and

$$\hat{K}_x = \frac{1}{k_0}\text{diag}(k_x + \vec{g}_x), \quad \hat{K}_y = \frac{1}{k_0}\text{diag}(k_y + \vec{g}_y), \tag{20}$$

where $\vec{g}_x$ and $\vec{g}_y$ are $1 \times N_g$ hypervectors of x and y projections of reciprocal lattice vectors. Matrix $\mathbb{A}[\hat{\alpha}^{\text{eff}}]$ also takes a simple form discussed in details in Appendix C.

The second most practical case is a lattice placed in close proximity of an interface between two homogeneous media. It should be noted, that even if the real particles lay right on the boundary, effective dipole lattice is placed at a level of the centers of these particles. Thus, for a dipole lattice situated at a distance of h above an interface, $\mathbb{B}$ matrices have the following form:

$$\mathbb{B}^{\text{in}} = \begin{bmatrix}e^{ik_0\hat{K}_z^{(1)}h_1} & \hat{0}\\ \mathbb{S}^{\text{int}}_{21}e^{ik_0\hat{K}_z^{(1)}(h_1+2h)} & \mathbb{S}^{\text{int}}_{22}e^{i(k_0\hat{K}_z^{(2)}(h_2-h)+k_0\hat{K}_z^{(1)}h)}\end{bmatrix},$$
$$\mathbb{B}^{\text{out}} = \begin{bmatrix}\mathbb{S}^{\text{int}}_{11}e^{i(k_0\hat{K}_z^{(2)}(h_2-h)+k_0\hat{K}_z^{(1)}h)} & \hat{0}\\ \mathbb{S}^{\text{int}}_{21}e^{ik_0\hat{K}_z^{(1)}(h_1+2h)} & -e^{ik_0\hat{K}_z^{(1)}h_1}\end{bmatrix}, \tag{21}$$

where $\mathbb{S}^{\text{int}}$ is the scattering matrix of the interface and operators $\hat{K}_z^{(1)}$ and $\hat{K}_z^{(2)}$ are calculated above and below the interface correspondingly, h_1 and h_2 are defined according to the Fig. 3(b).

The matrix $\mathbb{A}[\hat{\alpha}^{\text{eff}}]$ has the same form as for homogeneous environment (whereas $\hat{\alpha}^{\text{eff}}$ used for its calculation of course differs) since the plane of particle centers is fully inside a homogeneous medium.

It should be emphasized once again that the dyadic Green's function $\hat{G}$, which is used for a calculation of effective polarizability tensor $\hat{\alpha}^{\text{eff}}$, accounts for the structure of the layer (for

instance, presence of an interface) in the near field of metallic particles (see Appendix B). Indeed, this fact allows us not to account for the self-influence of dipoles by means of RCWA and escape from operating with all the high-$\mathbf{k}_\parallel$ harmonics. Also, it should be noted, that, although the matrices $\mathbb{A}[\hat{\alpha}^{\text{eff}}]$ of the same form are implemented for both considered cases they differ in tensors $\hat{\alpha}^{\text{eff}}$ applied for their calculation, which, in turn, strongly depend on the presence of an interface and a distance h to it.

There is an interesting fact that such splitting parameters as h^1 and h^2 can be chosen arbitrarily and even set to zero. However, the method performance is determined by the distance to the first boundary not accounted by the local scattering matrix. Indeed, the closer the boundary, the larger is the number of required harmonics and the less is our advantage over the conventional RCWA. Moreover, for distances of the order of the particle size, our approach becomes inapplicable and an additional boundary should be included in a local environment to be accounted by the polarizability tensor.

IV. EXAMPLE: HYBRID RESONANCES

Plasmonic metals play an important role in modern photonics, because of unique ability to enhance light-matter interaction via strong confinement of light in subwavelength dimensions. Very well-known localized surface plasmon resonances (LSPR) and surface plasmon resonances (SPR) have low Q factors but can compete with conventional resonances because of extremely small mode volume. In some cases, an intermediate regime of middle Q factor and mode volume is needed, which suggests the use of hybrid plasmon-photonic resonators [42,43]. An elegant way of implementation of this idea is a construction a regular lattice of resonant plasmonic nanoparticles. Such a structure allows employing both advantages and features of plasmonic and periodic structures. Lattice plasmon resonances that occur in them are actively implemented in biosensors [44–46], sources of light [36,47,48], and stretchable devices [49]. They might be used for lasing [50,51], strong coupling with emitting systems [52,53] and other purposes [54–56].

Plasmonic lattices have already been thoroughly studied theoretically. Such universal near-field methods as FEM or finite-difference time-domain method [57] (FDTD) can be implemented for a description of any periodic structure. However, they are too computationally expensive for observation of angle-dependent spectra with a good resolution, which requires at least thousands of computations. RCWA [13,19] specialized for periodic structures as it was mentioned before also fails in this case. Plasmonic lattices not only consist from small particles but generate high contrast in permittivities of adjacent materials as well. These factors together with exciting physical phenomena make them the most promising candidate for the first application of our approach.

For this reason, in order to show the performance of our method and illustrate the physical phenomena, which can be investigated, we consider plasmonic lattice in three different environments [see Figs. 4(a)–4(c)]. We have chosen a square lattice of silver nanodisks with a period of $a = 400$ nm. Disks have the radius of 30 nm, the height of 20 nm and are described by Johnson-Christy optical constants [58]. In the first case, this lattice is embedded in an infinite surrounding of silica ($\varepsilon = 2.1$). In the second variant of the structure, the lattice is incorporated directly in the middle of this waveguide. Also, in the latter one, we deposit nanoparticles on an 800-nm membrane silica waveguide.

A. Homogeneous environment

To start with we have calculated extinction spectra ($-\ln T$, where T is a transmission in the main diffraction order) of the plasmonic lattice in a bulk silica for both polarizations of light incident on a lattice along its crystallographic axis [see Figs. 4(d) and 4(g)]. Several specific phenomena are observed in this structure.

So-called Rayleigh anomalies [59] [magenta dashed lines in Figs. 4(d) and 4(g)] correspond to openings of different diffraction channels. In other words, for this relation of ω and $\mathbf{k}_\parallel$ all the particles radiate light coherently along the plane of a lattice, which results in in-phase contribution into the $\hat{C}$ tensor, its divergence and subsequent vanishing of the effective polarizability $\hat{\alpha}^{\text{eff}} \to 0$. Hence, in dipole approximation lattice becomes effectively transparent under Rayleigh condition, which is clearly seen in Figs. 4(d), 4(g) and 4(i). At the same time, when we go to the energies lower than Rayleigh anomalies, interaction constant $\hat{C}$ slightly decreases, which leads to a fulfillment of the resonant condition for LPRs, observed in Figs. 4(d), 4(g) and 4(i) as well. These resonances are so-called Fano-Wood anomalies [59], which occur when one of the diffraction orders matches both frequency and an in-plane component of the wave vector of the guided mode. LPRs in a homogeneous or almost homogeneous ambience have been thoroughly studied both theoretically and experimentally [35,45,54,60–62]. Their dispersion spectra have been observed experimentally and explained in Ref. [60]. Extinction spectra of the plasmonic lattice in a homogeneous environment are shown in Fig. 4(j). Reflection and transmission spectra, which can be potentially measured directly in the experiment as well as absorption and diffraction spectra of all the considered structures are presented in Ref. [63].

B. Lattice in a waveguide

When the lattice is embedded in the middle of the waveguide of finite thickness [see Fig. 4(b)] photonic guided modes come into play, while the positions of LSPR and LPR almost do not change. An interaction between plasmonic resonances with guided modes leads to an appearance of hybridized resonances [see Figs. 4(e), 4(h) and 4(k)], which represents the main difference with the lattice in the bulk space. Since the lattice is located strictly in the middle of the symmetric membrane waveguide the hybridization is determined by the parity of the guided modes. Therefore half of the modes, which have zero electric fields in the center of the waveguide are optically active.

The charachteristic example is observed for p-polarized wave at $\hbar\omega \approx 2.15$ eV and $k_x \approx 0.11 \times 2\pi/a$ [see Fig. 4(h)]. In this point, almost horizontal dispersion curve of lattice plasmon resonance is crossed by a second TM guided mode, which results in Rabi splitting.

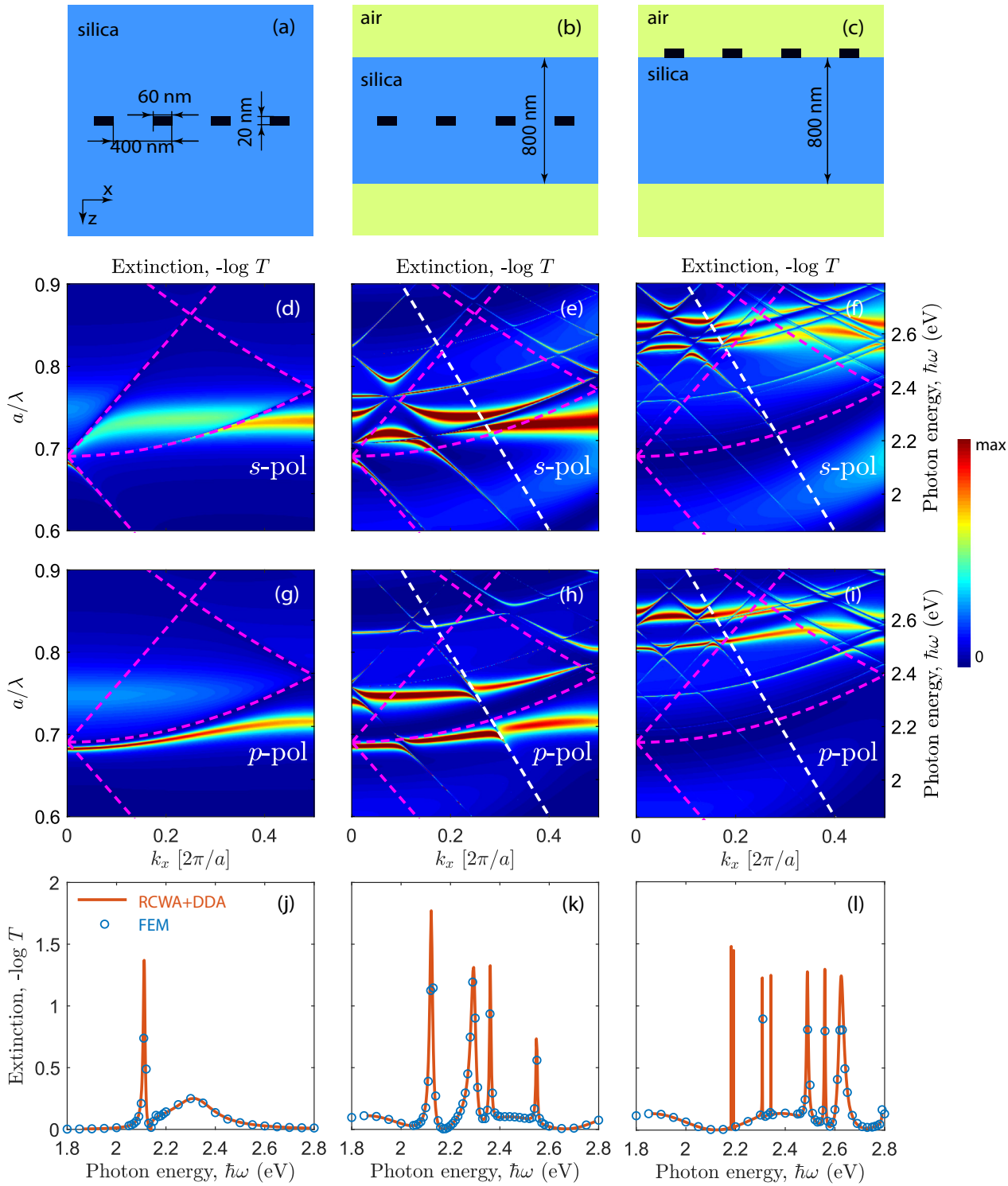

FIG. 4. Schematics of the plasmonic lattice in different environments [(a)–(c)]. In-plane wave-vector and energy dependencies of extinction ($-\ln T$, where T is a transmission in the main diffraction order) in s and p polarizations [(d)–(i)] for the case shown in (a)–(c) correspondingly. Color scale of (d)–(i) is explained on the right. (j)–(l) show extinction spectra for the normal incidence of light, which corresponds to a $k_x = 0$ section of angle-dependent spectra. They include the comparison of computations conducted via our approach with conventional FEM calculations.

C. Lattice on a waveguide

Despite the apparent similarity of the structures, the appearance of an interface in proximity of a lattice [see Fig. 4(c)] strongly changes optical properties. The difference comes from the fact that dipole located near an interface between two media almost does not radiate light along the boundary. It can be explained by the destructive interference of waves

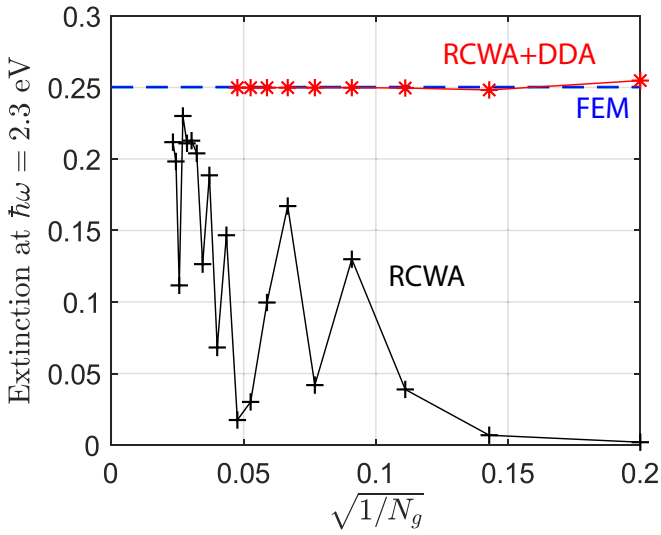

FIG. 5. Extinction of the lattice in bulk silica for a normally incident light at $\hbar\omega = 2.3$ eV calculated by different methods as a function of $\sqrt{1/N_g}$, where N_g is the total number of Fourier harmonics.

with their counterparts totally reflected in an opposite phase. Therefore, in this case, LSPRs are able to couple to each other only via near field, which strongly suppresses any collective phenomena. However, the feedback required for observation of Fano-Wood anomalies can emerge again from the coupling of LSPRs to an external photonic guided mode.

In this way, we observe coupling between strongly blueshifted LSPRs (see Appendix A) and guided photonic modes of a membrane silica waveguide [see Fig. 4(c)]. Since the lattice is located on the surface of the waveguide, guided modes of both parities are excited in the structure [see Figs. 4(f), 4(i) and 4(l)], unlike the previous case.

V. CONVERGENCE AND COMPARISON TO RCWA AND FEM

In order to verify the considered method, we compare our results with FEM calculations conducted in COMSOL MULTIPHYSICS. Since the calculation of extinction coefficients for each and every frequency and in-plain wave-vector component takes of the order of minute it is possible to conduct computations varying only one parameter in a reasonable time. We have considered spectra corresponding to a normal incidence of light on the same structures. As it can be seen from Figs. 4(j)–4(l), our results almost perfectly match with FEM calculations.

In order to compare convergence rate with conventional RCWA method, we have considered extinction emerging in the lattice in a homogeneous silica under the normal-incident light of 2.3 eV. It is seen in Fig. 5 that DDA enhanced method converges almost immediately, which is actually determined by the convergence rate of the dynamical interaction constant $\hat{C}(\mathbf{k}_\parallel)$ (see Appendix B for details). Concurrently, original RCWA method converges very slowly and does not provide reliable results even for 1681 harmonics, which is the maximum available value in our calculations.

VI. CONCLUSIONS

We have proposed a method for the implementation of DDA method in RCWA. Although, our approach is very general and allows considering lattices of nanoparticles in a complex environment, in this paper, we have implemented it for lattices in a homogeneous ambience and on a boundary between two homogeneous media, which are the most practical cases. We have demonstrated its operational feasibility by calculation of spectra for solitary plasmonic lattice and a lattice coupled with an optical waveguide. An occurrence of Fano-Wood anomalies, lattice plasmon resonances, and strong coupling between them is observed via the proposed approach. The accuracy of our approach was verified by comparison with FEM calculation, whereas convergence rate was shown to be much faster than in conventional RCWA calculations. Fast speed of calculation (typically several dozens of milliseconds for one computation at a fixed ω and $\mathbf{k}_\parallel$) and high accuracy of results makes this approach convenient and perspective for both interpretation of experimental results and fundamental analysis of phenomena occurring in plasmonic lattices. Although in this paper we formulate our method for a single particle in the unit cell, it can be easily generalized for the case of multiple particles.

ACKNOWLEDGMENT

This work was supported by the Russian Foundation for Basic Research (Grant No. 18-29-20032).

APPENDIX A: POLARIZABILITY TENSOR CALCULATION

In order to find a polarizability $\hat{\alpha}$ of an isolated nanoparticle, it is very convenient to switch to the total/scattered field formulation. Indeed, it can be easily shown that if $\mathbf{E}^{\mathrm{bg}}(\mathbf{r})$ is a solution of Maxwell's equations for the definite environment of a particle (without a particle itself) given by a permittivity distribution $\varepsilon^{\mathrm{bg}}(\mathbf{r})$, then the following calculation rule can be formulated. In the presence of an auxiliary scatterer (plasmonic nanoparticle in our case), the scattered field (defined as the difference between the total field and the background one) $\mathbf{E}^{\mathrm{sc}}(\mathbf{r}) = \mathbf{E}^{\mathrm{tot}}(\mathbf{r}) - \mathbf{E}^{\mathrm{bg}}(\mathbf{r})$ can be found as a radiation field of a distributed current $\mathbf{j}^{\mathrm{bg}}(\mathbf{r}) = -i\omega\Delta\varepsilon(\mathbf{r})\mathbf{E}^{\mathrm{bg}}(\mathbf{r})/(4\pi)$ [64,65], where $\Delta\varepsilon(\mathbf{r}) = \varepsilon^{\mathrm{tot}}(\mathbf{r}) - \varepsilon^{\mathrm{bg}}(\mathbf{r})$ is a difference of particle and background structure permittivities. The dipole moment, which we are searching for, corresponds to distribution of the free charges, which are placed in a medium described by $\varepsilon^{\mathrm{bg}}(\mathbf{r})$ permittivity and generate an additional field, which together with $\mathbf{E}^{\mathrm{bg}}$ constitute the total field $\mathbf{E}^{\mathrm{tot}}$. Therefore the density of the additional dipole moment can be found as $(\mathbf{D}^{\mathrm{tot}} - \varepsilon^{\mathrm{bg}}\mathbf{E}^{\mathrm{tot}})/(4\pi) = \Delta\varepsilon\mathbf{E}^{\mathrm{tot}}/(4\pi)$ [66], which brings us to the expression for dipole moment of a particle:

$$\mathbf{P} = \int \frac{\Delta\varepsilon}{4\pi}\mathbf{E}^{\mathrm{tot}}(\mathbf{r})d^3\mathbf{r} = \int \frac{\Delta\varepsilon}{4\pi}\left(\mathbf{E}^{\mathrm{bg}}(\mathbf{r}) + \mathbf{E}^{\mathrm{sc}}_{\mathbf{j}^{\mathrm{bg}}}(\mathbf{r})\right)d^3\mathbf{r}, \quad \text{(A1)}$$

Since, in this paper, we consider small particles in media with constant permittivity, $\varepsilon^{\mathrm{bg}}(\mathbf{r})$, over their volume (boundaries between materials does not intersect particles), we assume $\mathbf{E}^{\mathrm{bg}}(\mathbf{r})$ [not $\mathbf{E}^{\mathrm{sc}}(\mathbf{r})$] to be constant in space on the dimensions of a particle $\mathbf{E}^{\mathrm{bg}}(\mathbf{r}) = \mathbf{E}^{\mathrm{bg}}$. This means that the

primary induced current $\mathbf{j}^{\mathrm{bg}}(\mathbf{r})$ is just a vector with three components, not dependent on coordinates and makes it possible to introduce $\hat{\alpha}$ as a simple 3×3 tensor, connecting additional dipole moment of a particle, $\mathbf{P}$, with a background field $\mathbf{E}^{\mathrm{bg}}$:

$$\mathbf{P} = \hat{\alpha}\mathbf{E}^{\mathrm{bg}} = \frac{\Delta\varepsilon V}{4\pi}\left(\mathbf{E}^{\mathrm{bg}} + \left\langle \mathbf{E}^{\mathrm{sc}}_{\mathbf{j}^{\mathrm{bg}}} \right\rangle\right), \tag{A2}$$

where V is the volume of a particle and $\langle \mathbf{E}^{\mathrm{sc}}_{\mathbf{j}^{\mathrm{bg}}} \rangle$ is a scattered field (determined as a field generated by the current density $\mathbf{j}^{\mathrm{bg}}$) averaged over the volume of a particle. Such an approach clearly shows that dipole approximation can be applied even for a particle in a very complicated environment and provides an easy-to-apply procedure of $\hat{\alpha}$ tensor calculation for the cases considered in this paper.

Thus the only thing that should be done to calculate polarizability tensor, $\hat{\alpha}$, is the calculation of scattered field, which is a field radiated by an effective current density $\mathbf{j}^{\mathrm{bg}}$. Since, the connection between dipole moment and electric field is linear a unitary background field (e.g., $\mathbf{E}^{\mathrm{bg}} = [1, 0, 0]^T$) is taken in numerical simulations. In general case, three independent calculations are required to determine the response of a particle on each polarization of a background field. However, in the presence of additional symmetry, there can be only two or even one independent components, which simplifies calculations additionally. We conduct the described calculations in COMSOL MULTIPHYSICS, whereas they might be potentially realized via any near-field calculation methods.

In Fig. 6, we show energy dependence of in-plain component $\hat{\alpha}_{xx}$ of a polarizability tensor of a nanodisk in bulk silica, air and in the air on the air/silica interface. It is seen, that wide resonances of LSPRs correlate with the obtained spectra [see Figs. 4(d)–4(i)]. Since silica has permittivity higher than air, corresponding plasmonic resonance in a disk is strongly red shifted. Resonance of a particle laying on a boundary is obviously located between them. Almost perfect matching of extinction spectra with FEM calculations [see Figs. 4(j)–4(l)] indirectly proves that our approach provides precise results and substantiates our choice.

There are several important advantages of the method applied for the calculation of $\hat{\alpha}$ tensor. First of all, it is very universal so that allows considering particles of any, even very complex shape, in any environment. Also, it provides high accuracy, which as a result leads to high-precision spectra.

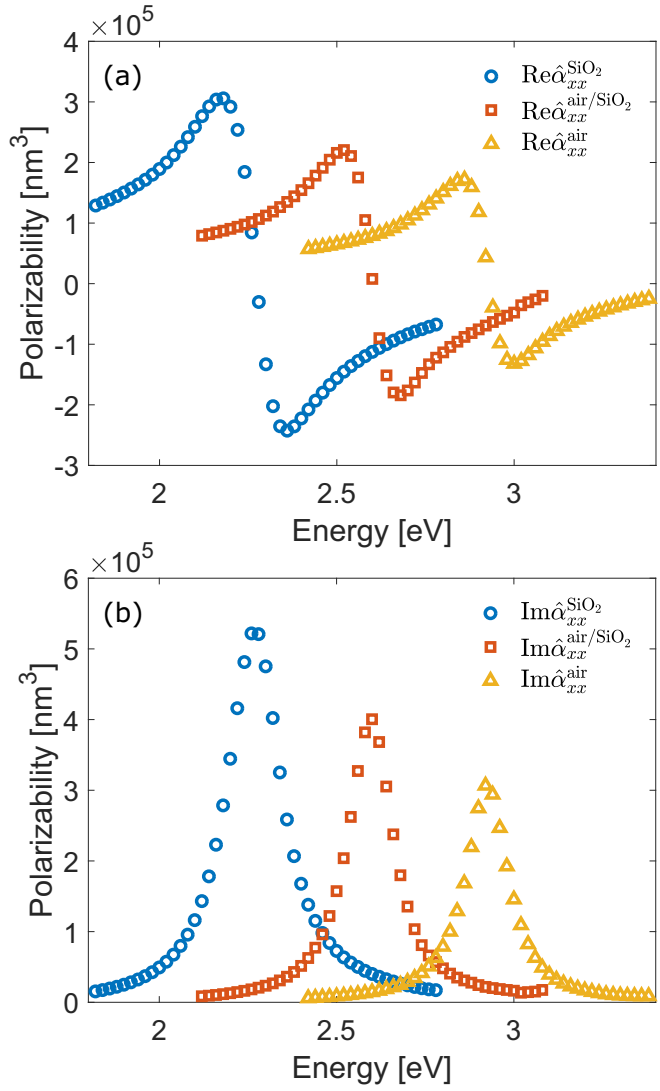

FIG. 6. Energy dependence of real (a) and imaginary (b) parts of in-plain polarizability of the same silver nanodisks embedded in bulk silica, air and laying on the air/silica interface. All the data is calculated in COMSOL MULTIPHYSICS.

APPENDIX B: SUM CALCULATION

1. Green's function filtering

First of all, since in this paper we consider only examples of environments, which have translational symmetry in the x-y plane, and all the particles are located in the same plane, for a fixed z coordinate, Green's function depends only on the difference of coordinates. Therefore sum (4) transforms to a slightly simpler form:

$$\hat{C}(\mathbf{k}_\parallel) = \sum_{j \neq 0} \hat{G}(\mathbf{t}_j, z = z_p) e^{i\mathbf{k}_\parallel \mathbf{t}_j}, \tag{B1}$$

where $\mathbf{t}_j$ is the jth translational vector of a lattice in real space.

Typically this sum converges very slowly. For instance, in a homogeneous medium dyadic Green's function $\hat{G}_{\alpha\beta}(\mathbf{r}) = k_0^2(\delta_{\alpha\beta} + \frac{1}{k^2}\partial_\alpha\partial_\beta)\frac{e^{ikr}}{r}$ (where $k = \sqrt{\varepsilon}_m k_0$ is a wave vector in a medium) decays as e^{ikr}/r, which makes the sum calculation not a trivial problem. Various methods have been developed for an efficient calculation of a lattice sum for homogeneous ambience [37,67–70]. Many of them, starting from the classical Ewald's method are based on the following idea: if a lattice sum of a function converges slowly in real space, then this function can be represented as a sum of two auxiliary functions. The first one accounts for high gradients and decays very fast at infinity, whereas the second one, on the contrary, should be very smooth. In this way, the sum of the first function converges fast in real space and the sum of the second one can be calculated efficiently in reciprocal space (via the Poisson formula [71]).

Following this idea, we implement a very similar method, which helps us to obtain fast convergence for lattices both in homogeneous ambience and on an interface between two media and has very clear physical sense. Green's function has

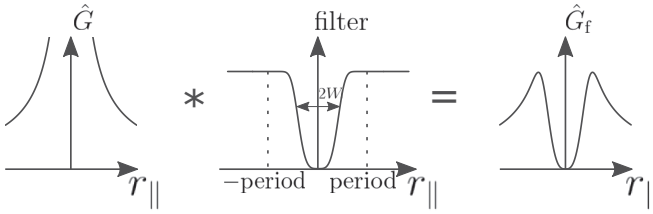

FIG. 7. Schematic of filtering of the dyadic Green's function. W is the width of the filter, which should be less than a period.

high gradients only in the proximity of the zero point, but in our case, this point is not included in the sum, since self-action of a particle is already accounted for by the polarizability tensor $\hat{\alpha}$. This fact gives us an opportunity to split the Green's function in such a way that the contribution of the first, high-gradient function is negligible. In order to do that, we multiply the original Green's function by a special filter, which is equal to zero at the zero point and tends to unity for distances larger or equal to the period of a structure $\hat{G}_f(\mathbf{r}) = f(\mathbf{r})\hat{G}(\mathbf{r})$ (see Fig. 7). In this way, the summation can be conducted over all the nodes of a lattice, having exactly the same result:

$$\hat{C}(\mathbf{k}_\parallel) = \sum_{j\neq 0} \hat{G}(\mathbf{t}_j) e^{-i\mathbf{k}_\parallel \mathbf{t}_j} = \sum_j \hat{G}_f(\mathbf{t}_j) e^{-i\mathbf{k}_\parallel \mathbf{t}_j} = \frac{4\pi^2}{s} \sum_j \hat{M}_f(\mathbf{k}_\parallel + \mathbf{g}_j), \quad \text{(B2)}$$

where $\hat{M}_f(\mathbf{k}_\parallel) = \frac{1}{4\pi^2} \int \hat{G}_f(\mathbf{r}) e^{-i\mathbf{k}_\parallel \mathbf{r}} d^2\mathbf{r}$, is the filtered dyadic Green's function in reciprocal space, s is an area of a unit cell in real space and $\mathbf{g}_j$ is a jth vector of reciprocal lattice. If the filtered Green's function, $\hat{G}_f$, is a smooth enough that it has n derivatives and all of them are absolutely integrable, then its Fourier image $\hat{M}_f(\mathbf{k}_\parallel) = o(k_\parallel^{-n})$ for $k_\parallel \to \infty$, which provides fast asymptotic convergence.

This simple approach not only provides fast convergence but also has a clear physical meaning. Indeed, if we apply a filter, which is smooth, then each summand in reciprocal space has a sense of a contribution of corresponding diffraction order in the interaction between particles. Therefore, in most cases, it is possible to account for the same number of diffraction orders in sum calculation and in the scattering matrix $\mathbb{S}$, which is very convenient.

However, calculation of Fourier image of a filtered Green's function $\hat{M}_f(\mathbf{k}_\parallel)$ is not always an easy task. When the homogeneous space is considered, then it is possible to compose such a filtering function, that Fourier transform can be calculated analytically. However, when a particle near an interface is considered, then expressions become too complex. Since in real space filtering is just a multiplication then in reciprocal space we deal with a convolution $\hat{M}_f(\mathbf{k}_\parallel) = (F * \hat{M})(\mathbf{k}_\parallel)$, where $F(\mathbf{k}_\parallel) = \frac{1}{4\pi^2} \int f(\mathbf{r}_\parallel) e^{-i\mathbf{k}_\parallel \mathbf{r}} d^2\mathbf{r}$ and $\hat{M}(\mathbf{k}_\parallel) = \frac{1}{4\pi^2} \int \hat{G}(\mathbf{r}_\parallel) e^{-i\mathbf{k}_\parallel \mathbf{r}_\parallel} d^2\mathbf{r}_\parallel$. However, since filtering function tends to unity at infinity, it is convenient to introduce complementary filtering function, $\bar{f}(\mathbf{r}_\parallel) = 1 - f(\mathbf{r}_\parallel)$, for further derivations. In this way, we introduce $\hat{M}_{\bar{f}}(\mathbf{k}_\parallel) = (\bar{F} * \hat{M})(\mathbf{k}_\parallel)$, which helps to find the originally filtered Green's function as $\hat{M}_f(\mathbf{k}_\parallel) = \hat{M}(\mathbf{k}_\parallel) - \hat{M}_{\bar{f}}(\mathbf{k}_\parallel)$.

2. Green's function near an interface

Here, we consider Green's function for an emitter located in the proximity of an interface between two media since it might be easily reduced to a case of a homogeneous medium. It is known, that this function can be expressed as a sum of two parts, $\hat{M} = \hat{M}^0 + \hat{M}^r$ [72]. The first term is just Green's function of the homogeneous medium and the second one accounts for the field reflected from the boundary, which is naturally calculated in reciprocal space because it requires just multiplication of amplitudes of plane waves by Fresnel coefficients.

Green's function for a homogeneous ambience in reciprocal space $\hat{M}^0(\mathbf{k}_\parallel)$ can be expressed as a sum of s- and p-polarized contributions:

$$\hat{M}^{0,\pm} = \hat{M}_s^{0,\pm} + \hat{M}_p^{0,\pm} = \frac{ik_0^2}{2\pi k_z k_\parallel^2} \begin{pmatrix} k_y^2 & -k_x k_y & 0 \\ -k_x k_y & k_x^2 & 0 \\ 0 & 0 & 0 \end{pmatrix} + \frac{ik_0^2}{2\pi k^2 k_\parallel^2} \begin{pmatrix} k_x^2 k_z & k_x k_y k_z & \mp k_x k_\parallel^2 \\ k_x k_y k_z & k_y^2 k_z & \mp k_y k_\parallel^2 \\ \mp k_x k_\parallel^2 & \mp k_y k_\parallel^2 & k_\parallel^4 / k_z \end{pmatrix}, \quad \text{(B3)}$$

where $k_z = \sqrt{k^2 - \mathbf{k}_\parallel^2}$ is the z component of the wave vector (positive imaginary part should be chosen for $k_\parallel > k$). Sign $\pm$ corresponds to upper/lower half-spaces, however, when we consider plane $z = z_p$, the choice of the sign does not matter and all the alternating-sign components finally do not make any contribution.

Splitting of the tensor into two terms corresponding to different polarizations is very convenient for an accounting of reflection from an interface. We just have to multiply each term by corresponding reflection coefficient, choose appropriate signs keeping in mind the fact that the reflected wave propagates in the direction opposite to an incident one and take into account an additional phase, which is gained during the propagation to the interface and back.

Without loss of generality, we consider a lattice of particles placed above an interface, whose centers are located at a distance of h from a boundary [see Fig. 3(b)]. Reflected part of Green's function has the following form:

$$\hat{M}^r = \hat{M}_s^r + \hat{M}_p^r = e^{2ik_z h} \left[r_s(k_\parallel) \frac{ik_0^2}{2\pi k_z k_\parallel^2} \begin{pmatrix} k_y^2 & -k_x k_y & 0 \\ -k_x k_y & k_x^2 & 0 \\ 0 & 0 & 0 \end{pmatrix} - r_p(k_\parallel) \frac{ik_0^2}{2\pi k^2 k_\parallel^2} \begin{pmatrix} k_x^2 k_z & k_x k_y k_z & k_x k_\parallel^2 \\ k_x k_y k_z & k_y^2 k_z & k_y k_\parallel^2 \\ -k_x k_\parallel^2 & -k_y k_\parallel^2 & -k_\parallel^4 / k_z \end{pmatrix} \right], \quad \text{(B4)}$$

where r_s and r_p are Fresnel reflection coefficients for corresponding polarizations, and $e^{2ik_z h}$ is a phase delay.

3. Fast calculation of convolution

2D convolution, which is required for filtering of $\hat{M}$ is a rather expensive operation. In order to tackle this problem, we boost it in several ways.

It can be easily noticed, that components of of all the $\hat{M}$ tensor summands have some trivial angular dependence. Here, we consider axial symmetric filtering functions $\bar{f}(r_\parallel)$, which means that $\bar{F}(k_\parallel)$ also depends only on the absolute value of the wave-vector in-plain component. This makes it possible to reduce the convolution to a much simpler form.

Indeed, let us consider a convolution for a certain component of the tensor $m_{\bar{f}}(\mathbf{k}_\parallel) = (\bar{F} * m)(\mathbf{k}_\parallel)$. From the explicit expressions for tensor components, it can be easily noticed, that any of them can be represented in the following way:

$$m(k_\parallel, \alpha) = m_k(k_\parallel) m_\alpha(\alpha), \tag{B5}$$

where angular part takes one of the following forms:

$$m_\alpha(\alpha) = \left\{ \begin{array}{c} 1(\alpha) \\ \sin\alpha \\ \cos\alpha \\ \sin^2\alpha \\ \cos^2\alpha \\ \sin\alpha\cos\alpha \end{array} \right\}. \tag{B6}$$

In this way, convolution can be calculated as follows:

$$\begin{aligned} m_{\bar{f}}(k_\parallel, \alpha) &= \int m_k(k'_\parallel) m_\alpha(\alpha') \\ &\quad \times \bar{F}\left(\sqrt{k_\parallel^2 + k_\parallel'^2 - 2k'_\parallel k_\parallel \cos(\alpha' - \alpha)}\right) k'_\parallel dk'_\parallel d\alpha' \\ &= \int m_k(k'_\parallel) m_\alpha(\alpha' + \alpha) \\ &\quad \times \bar{F}\left(\sqrt{k_\parallel^2 + k_\parallel'^2 - 2k'_\parallel k_\parallel \cos(\alpha')}\right) k'_\parallel dk'_\parallel d\alpha'. \end{aligned} \tag{B7}$$

For each and every element of a set m_α, a decomposition of $m_\alpha(\alpha' + \alpha)$ can be conducted. To give an example, a case of $m_\alpha(\alpha) = \sin^2(\alpha)$ is considered below. Since $\sin^2(\alpha + \alpha') = 0.5 - 0.5\cos(2\alpha)\cos(2\alpha') + 0.5\sin(2\alpha)\sin(2\alpha')$, we obtain

$$\begin{aligned} m_{\bar{f}}(k_\parallel, \alpha) &= 0.5\mathfrak{m}(k_\parallel) - 0.5\cos(2\alpha)\mathfrak{m}_{\cos 2\alpha}(k_\parallel) \\ &\quad + 0.5\sin(2\alpha)\mathfrak{m}_{\sin 2\alpha}(k_\parallel), \end{aligned} \tag{B8}$$

where

$$\begin{aligned} \mathfrak{m}(k_\parallel) &= \int m_k(k'_\parallel) \bar{F}\left(\sqrt{k_\parallel^2 + k_\parallel'^2 - 2k'_\parallel k_\parallel \cos(\alpha')}\right) \\ &\quad \times k'_\parallel dk'_\parallel d\alpha', \end{aligned} \tag{B9}$$

$$\begin{aligned} \mathfrak{m}_{\sin 2\alpha}(k_\parallel) &= \int m_k(k'_\parallel) \sin(2\alpha') \bar{F}\left(\sqrt{k_\parallel^2 + k_\parallel'^2 - 2k'_\parallel k_\parallel \cos(\alpha')}\right) \\ &\quad \times k'_\parallel dk'_\parallel d\alpha', \end{aligned} \tag{B10}$$

$$\begin{aligned} \mathfrak{m}_{\cos 2\alpha}(k_\parallel) &= \int m_k(k'_\parallel) \cos(2\alpha') \bar{F}\left(\sqrt{k_\parallel^2 + k_\parallel'^2 - 2k'_\parallel k_\parallel \cos(\alpha')}\right) \\ &\quad \times k'_\parallel dk'_\parallel d\alpha'. \end{aligned} \tag{B11}$$

In this way, for a definite frequency, $k_\parallel$ dependence might be calculated on a grid and then interpolated. The fact that angular dependence is determined analytically and all precalculations are conducted for a 1D grid as well as the possibility not to calculate functions many times in closely spaced points increase the speed of computations drastically. The strongest speedup is observed when the angle dependence of a spectrum is considered. Moreover, for some filters, angular part of integrals (B9)–(B11) and similar ones can be calculated analytically, which additionally speeds the calculations up.

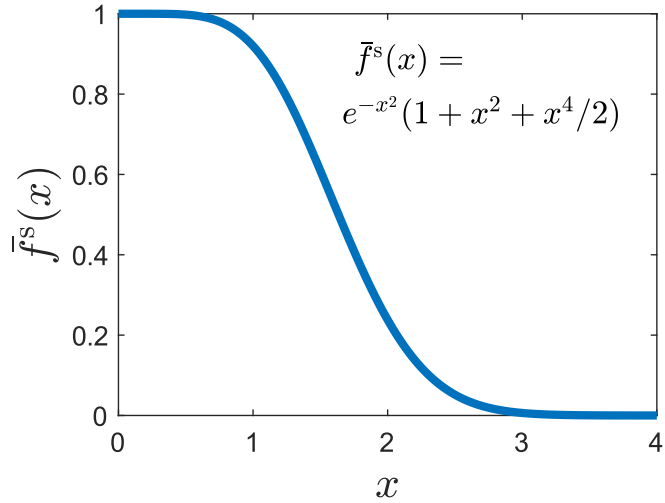

FIG. 8. Graph of the filtering function $\bar{f}^s(x)$.

Hereinafter, we observe a specific filter of the following shape $\bar{f}^s(x) = e^{-x^2}(1 + x^2 + x^4/2)$ (see Fig. 8), which we use in our calculations. This filter is convenient for a practical utilization because of a high rate of decay and the possibility to operate with it analytically, which is demonstrated below. Its width can be roughly estimated as $\int_0^\infty \bar{f}^s(x)dx = 15\sqrt{\pi}/16 \approx 1.66$. Therefore, in order to obtain the filter of the provided width, W (see Fig. 7), we should use $\bar{f}(r_\parallel) = \bar{f}^s(1.66 r_\parallel / W)$. Since original Green's function diverges as $r_\parallel^{-3}$ at the zero point and filter $f(r_\parallel)$ decays as $r_\parallel^6$, then the filtered Green's function has to have at least two derivatives and therefore $\hat{M}_f(\mathbf{k}_\parallel) = o(1/k_\parallel^2)$ for $k_\parallel \to \infty$.

Fourier image of the filter $\bar{f}^s(x)$ can be easily calculated analytically:

$$\begin{aligned} \bar{F}^s(y) &= \frac{1}{4\pi^2} \int_0^\infty dx \left[x\bar{f}^s(x) \int_0^{2\pi} d\varphi e^{-xy\cos\varphi} \right] \\ &= e^{-y^2/4}(96 - 24y^2 + y^4)/(128\pi). \end{aligned} \tag{B12}$$

At the same time, Fourier image of the original filter $\bar{f}(r_\parallel)$ is subsequently derived as $\bar{F}(\mathbf{k}_\parallel) = \bar{F}^s(\mathbf{k}_\parallel W/1.66)$.

The following expressions are valid for the particular filter utilized in this paper:

$$\begin{aligned} &\int \bar{F}\left(\sqrt{k_\parallel^2 + k_\parallel'^2 - 2k'_\parallel k_\parallel \cos(\alpha')}\right) d\alpha' \\ &= [(\kappa_\parallel^4 + \kappa_\parallel'^4 + 6\kappa_\parallel^2\kappa_\parallel'^2 - 24(\kappa_\parallel'^2 + \kappa_\parallel^2) + 96) I_0(\kappa_\parallel\kappa'_\parallel/2) \\ &\quad - 4\kappa_\parallel\kappa'_\parallel(\kappa_\parallel^2 + \kappa_\parallel'^2 - 10) I_1(\kappa_\parallel\kappa'_\parallel/2)] e^{-(\kappa_\parallel^2 + \kappa_\parallel'^2)/4}/64, \end{aligned} \tag{B13}$$

$$\int \sin(2\alpha')\bar{F}\left(\sqrt{k_\parallel^2 + k_\parallel'^2 - 2k_\parallel' k_\parallel \cos(\alpha')}\right)d\alpha' = 0, \quad \text{(B14)}$$

$$\int \cos(2\alpha')\bar{F}\left(\sqrt{k_\parallel^2 + k_\parallel'^2 - 2k_\parallel' k_\parallel \cos(\alpha')}\right)d\alpha'$$
$$= \Big[(\kappa_\parallel^4 + \kappa_\parallel'^4 + 6\kappa_\parallel^2\kappa_\parallel'^2 - 8(\kappa_\parallel^2 + \kappa_\parallel'^2))I_0(\kappa_\parallel\kappa_\parallel'/2)$$
$$- 4(\kappa_\parallel^4 + \kappa_\parallel'^4 - 8(\kappa_\parallel^2 + \kappa_\parallel'^2) + \kappa_\parallel^2\kappa_\parallel'^2(\kappa_\parallel^2 + \kappa_\parallel'^2 - 4))$$
$$\times \frac{I_1(\kappa_\parallel\kappa_\parallel'/2)}{\kappa_\parallel\kappa_\parallel'}\Big]e^{-(\kappa_\parallel^2+\kappa_\parallel'^2)/4}/64, \quad \text{(B15)}$$

$$\int \sin(\alpha')\bar{F}\left(\sqrt{k_\parallel^2 + k_\parallel'^2 - 2k_\parallel' k_\parallel \cos(\alpha')}\right)d\alpha' = 0, \quad \text{(B16)}$$

$$\int \cos(\alpha')\bar{F}\left(\sqrt{k_\parallel^2 + k_\parallel'^2 - 2k_\parallel' k_\parallel \cos(\alpha')}\right)d\alpha'$$
$$= [(\kappa_\parallel^4 + \kappa_\parallel'^4 + 6\kappa_\parallel^2\kappa_\parallel'^2 - 32(\kappa_\parallel^2 + \kappa_\parallel'^2) + 192)I_1(\kappa_\parallel\kappa_\parallel'/2)$$
$$- 4\kappa_\parallel\kappa_\parallel'(\kappa_\parallel^2 + \kappa_\parallel'^2 - 10)I_2(\kappa_\parallel\kappa_\parallel'/2)]e^{-(\kappa_\parallel^2+\kappa_\parallel'^2)/4}/64, \quad \text{(B17)}$$

where I_0, I_1, and I_2 are Bessel functions of corresponding orders, $\kappa = k_\parallel W/1.66$ and $\kappa' = k_\parallel' W/1.66$.

To conclude, in order to find a filtered Green's function in reciprocal space, $\hat{M}_f(\mathbf{k}_\parallel)$, at any point, we should calculate just several functions on a 1D grid and continue them analytically to the whole plane. Precalculation of this auxiliary functions on a grid and subsequent interpolation makes these computations much faster. Moreover, for specific filtering functions, calculation of angular part of an integral can be conducted analytically, which boosts calculations additionally.

Finally, this approach, allows us to calculate angle-dependent spectra in a few minutes on a regular laptop, which is more than enough for practical utilization. Moreover, calculation of convolution is even not a bottleneck in our calculations and does not limit the performance of the whole program.

APPENDIX C: DETAILS ON RCWA MATRIX CALCULATIONS

1. Combination of scattering matrices

The elements of the scattering matrix $\mathbb{S}$ which is a combination of two scattering matrices $\mathbb{S}^1$ and $\mathbb{S}^2$ denoted as $\mathbb{S} = \mathbb{S}^1 \otimes \mathbb{S}^2$ is given by the following formula:

$$\mathbb{S}_{11} = \mathbb{S}^2_{11}\left(\hat{I} - \mathbb{S}^1_{12}\mathbb{S}^2_{21}\right)^{-1}\mathbb{S}^1_{11}, \quad \text{(C1)}$$

$$\mathbb{S}_{12} = \mathbb{S}^2_{12} + \mathbb{S}^2_{11}\left(\hat{I} - \mathbb{S}^1_{12}\mathbb{S}^2_{21}\right)^{-1}\mathbb{S}^1_{12}\mathbb{S}^2_{22}, \quad \text{(C2)}$$

$$\mathbb{S}_{21} = \mathbb{S}^1_{21} + \mathbb{S}^1_{22}\left(\hat{I} - \mathbb{S}^2_{21}\mathbb{S}^1_{12}\right)^{-1}\mathbb{S}^2_{21}\mathbb{S}^1_{11}, \quad \text{(C3)}$$

$$\mathbb{S}_{22} = \mathbb{S}^1_{22}\left(\hat{I} - \mathbb{S}^2_{21}\mathbb{S}^1_{12}\right)^{-1}\mathbb{S}^2_{22}. \quad \text{(C4)}$$

2. Method of oscillating currents

The RCWA formalism allows to calculate the emission of oscillating dipoles embedded in an arbitrary layer. The basic principle to do that is to construct the amplitude discontinuity vector which connects the vectors of amplitudes at coordinates infinitesimally above and below the dipole plane [40]:

$$\begin{bmatrix}\vec{\mathrm{d}}\\ \vec{\mathrm{u}}\end{bmatrix}_{z_p+0} - \begin{bmatrix}\vec{\mathrm{d}}\\ \vec{\mathrm{u}}\end{bmatrix}_{z_p-0} = \begin{bmatrix}\vec{\mathrm{j}}_d\\ \vec{\mathrm{j}}_u\end{bmatrix} = \mathbb{A}\begin{bmatrix}\vec{\mathrm{d}}_0\\ \vec{\mathrm{u}}_0\end{bmatrix}. \quad \text{(C5)}$$

In this paper, we consider only examples, when the currents are located in a section of homogeneous layer (which does not exclude existence of other layers in near field slightly higher and lower), therefore all the derivations below are conducted under this assumption. Application of the material matrix $\mathbb{F}$ [13] to Eq. (C5) gives us jumps of tangential components of electric and magnetic fields:

$$\begin{bmatrix}E_x\\ E_y\\ H_x\\ H_y\end{bmatrix}_{z_p+0} - \begin{bmatrix}E_x\\ E_y\\ H_x\\ H_y\end{bmatrix}_{z_p-0} = \begin{bmatrix}J_{Ex}\\ J_{Ey}\\ J_{Hx}\\ J_{Hy}\end{bmatrix} = J = \mathbb{F}\begin{bmatrix}\vec{\mathrm{j}}_d\\ \vec{\mathrm{j}}_u\end{bmatrix}, \quad \text{(C6)}$$

where J is the vector of discontinuities of Fourier components of electric and magnetic fields. The elements of this vector are found from the Fourier components of the surface current **i** [40]:

$$\begin{bmatrix}J_{Ex}\\ J_{Ey}\end{bmatrix} = \frac{4\pi}{c\varepsilon}\begin{pmatrix}\hat{K}_x\\ \hat{K}_y\end{pmatrix}i_z, \qquad \begin{bmatrix}J_{Hx}\\ J_{Hy}\end{bmatrix} = \frac{4\pi}{c}\begin{pmatrix}i_y\\ -i_x\end{pmatrix}, \quad \text{(C7)}$$

where $\hat{K}_x$ and $\hat{K}_y$ are defined by formulas (20).

In this way, in order to find the matrix $\mathbb{A}$, we should just express harmonics of this current through the vector $[\vec{\mathrm{d}}_0, \vec{\mathrm{u}}_0]^T$. The first step is the application of the material matrix, which gives us fields:

$$\begin{bmatrix}E_x^0\\ E_y^0\\ H_x^0\\ H_y^0\end{bmatrix} = \mathbb{F}\begin{bmatrix}\vec{\mathrm{d}}_0\\ \vec{\mathrm{u}}_0\end{bmatrix}. \quad \text{(C8)}$$

This vector of electric and magnetic fields harmonics is consequently transformed to the vector of Fourier harmonics of all the components of electric field:

$$\begin{bmatrix}E_x^0\\ E_y^0\\ E_z^0\end{bmatrix} = \begin{bmatrix}\hat{I} & \hat{0} & \hat{0} & \hat{0}\\ \hat{0} & \hat{I} & \hat{0} & \hat{0}\\ \hat{0} & \hat{0} & \hat{K}_y/\varepsilon & -\hat{K}_x/\varepsilon\end{bmatrix}\begin{bmatrix}E_x^0\\ E_y^0\\ H_x^0\\ H_y^0\end{bmatrix}. \quad \text{(C9)}$$

In turn, this vector is used for calculation of electric field in real space at the position of the ith particle:

$$\mathbf{E}^0 = \begin{bmatrix}\mathrm{E}_x^0\\ \mathrm{E}_y^0\\ \mathrm{E}_z^0\end{bmatrix} = \begin{bmatrix}\vec{\Gamma} & \vec{0} & \vec{0}\\ \vec{0} & \vec{\Gamma} & \vec{0}\\ \vec{0} & \vec{0} & \vec{\Gamma}\end{bmatrix}\begin{bmatrix}E_x^0\\ E_y^0\\ E_z^0\end{bmatrix}, \quad \text{(C10)}$$

where $1 \times N_g$ hypervector $\vec{\Gamma}$ is set by the following expression:

$$\vec{\Gamma} = \exp(i(k_x + \vec{g}_x)x + i(k_y + \vec{g}_y)y), \tag{C11}$$

where (x, y) is the coordinate of a nanoparticle in the unit cell in a real space.

Thus, the current of the ith particle is determined as

$$\mathbf{I} = -i\omega\hat{\alpha}^{\text{eff}}\mathbf{E}^0. \tag{C12}$$

Finally, according to the Poisson formula a grid of point currents in real space corresponds to the following harmonics in Fourier space:

$$\begin{bmatrix} i_x \\ i_y \\ i_z \end{bmatrix} = \frac{1}{s}\begin{bmatrix} \vec{\Gamma} & \vec{0} & \vec{0} \\ \vec{0} & \vec{\Gamma} & \vec{0} \\ \vec{0} & \vec{0} & \vec{\Gamma} \end{bmatrix}^{\dagger}\begin{bmatrix} \mathrm{I}_x \\ \mathrm{I}_y \\ \mathrm{I}_z \end{bmatrix}, \tag{C13}$$

where s is a surface of a unit cell in a real space and dagger denotes Hermitian conjugate.

Combining Eqs. (C5)–(C13), we obtain the following expression for $\mathbb{A}$ tensor:

$$\mathbb{A} = \mathbb{F}^{-1}\hat{A}\mathbb{F}, \tag{C14}$$

where

$$\hat{A} = \frac{-4\pi i k_0}{s}\begin{bmatrix} \hat{0} & \hat{0} & \hat{K}_x/\varepsilon \\ \hat{0} & \hat{0} & \hat{K}_y/\varepsilon \\ \hat{0} & \hat{I} & \hat{0} \\ -\hat{I} & \hat{0} & \hat{0} \end{bmatrix}\begin{bmatrix} \vec{\Gamma} & \vec{0} & \vec{0} \\ \vec{0} & \vec{\Gamma} & \vec{0} \\ \vec{0} & \vec{0} & \vec{\Gamma} \end{bmatrix}^{\dagger} \times \hat{\alpha}^{\text{eff}}\begin{bmatrix} \vec{\Gamma} & \vec{0} & \vec{0} \\ \vec{0} & \vec{\Gamma} & \vec{0} \\ \vec{0} & \vec{0} & \vec{\Gamma} \end{bmatrix}\begin{bmatrix} \hat{I} & \hat{0} & \hat{0} & \hat{0} \\ \hat{0} & \hat{I} & \hat{0} & \hat{0} \\ \hat{0} & \hat{0} & \hat{K}_y/\varepsilon & -\hat{K}_x/\varepsilon \end{bmatrix}. \tag{C15}$$

[1] V. P. Bykov, ZhETF **62**, 505 (1972) [J. Exp. Theor. Phys. **35**, 269 (1972)].
[2] E. Yablonovitch, J. Opt. Soc. Am. B **10**, 283 (1993).
[3] K. Sakoda, *Optical Properties of Photonic Crystals*, Springer Series in Optical Sciences Vol. 80 (Springer Science & Business Media, Berlin, Heidelberg, 2004).
[4] R. W. Wood, Philos. Mag. **4**, 396 (1902).
[5] J. W. Strutt, Proc. R. Soc. Lond. A **79**, 399 (1907).
[6] U. Fano, JOSA **31**, 213 (1941).
[7] U. Fano, Phys. Rev. **124**, 1866 (1961).
[8] B. A. Munk, *Frequency Selective Surfaces: Theory and Design* (John Wiley & Sons, New York, 2005).
[9] R. Adato, A. A. Yanik, J. J. Amsden, D. L. Kaplan, F. G. Omenetto, M. K. Hong, S. Erramilli, and H. Altug, Proc. Natl. Acad. Sci. USA **106**, 19227 (2009).
[10] D. Dregely, R. Taubert, J. Dorfmüller, R. Vogelgesang, K. Kern, and H. Giessen, Nat. Commun. **2**, 267 (2011).
[11] A. Christ, S. G. Tikhodeev, N. A. Gippius, J. Kuhl, and H. Giessen, Phys. Rev. Lett. **91**, 183901 (2003).
[12] H. Benisty, D. Labilloy, C. Weisbuch, C. Smith, T. Krauss, D. Cassagne, A. Beraud, and C. Jouanin, Appl. Phys. Lett. **76**, 532 (2000).
[13] S. G. Tikhodeev, A. L. Yablonskii, E. A. Muljarov, N. A. Gippius, and T. Ishihara, Phys. Rev. B **66**, 045102 (2002).
[14] N. Yu and F. Capasso, Nat. Mater. **13**, 139 (2014).
[15] Q. Wang, E. T. Rogers, B. Gholipour, C.-M. Wang, G. Yuan, J. Teng, and N. I. Zheludev, Nat. Photonics **10**, 60 (2016).
[16] A. V. Kildishev, A. Boltasseva, and V. M. Shalaev, Science **339**, 1232009 (2013).
[17] G. Li, S. Zhang, and T. Zentgraf, Nat. Rev. Mater. **2**, 17010 (2017).
[18] S. A. Dyakov, V. A. Semenenko, N. A. Gippius, and S. G. Tikhodeev, Phys. Rev. B **98**, 235416 (2018).
[19] M. Moharam, E. B. Grann, D. A. Pommet, and T. Gaylord, J. Opt. Soc. Am. A **12**, 1068 (1995).
[20] J. W. Gibbs, Nature (London) **59**, 200 (1898).
[21] E. Hewitt and R. E. Hewitt, Arch. Hist. Exact Sci. **21**, 129 (1979).
[22] L. Li, J. Opt. Soc. Am. A **14**, 2758 (1997).
[23] G. Granet and J.-P. Plumey, J. Opt. A: Pure Appl. Opt. **4**, S145 (2002).
[24] T. Weiss, G. Granet, N. A. Gippius, S. G. Tikhodeev, and H. Giessen, Opt. Express **17**, 8051 (2009).
[25] P. C. Chaumet, A. Rahmani, and G. W. Bryant, Phys. Rev. B **67**, 165404 (2003).
[26] N. Meinzer, W. L. Barnes, and I. R. Hooper, Nat. Photonics **8**, 889 (2014).
[27] W. Zhou and T. W. Odom, Nat. Nanotechnol. **6**, 423 (2011).
[28] C. F. Bohren and D. R. Huffman, *Absorption and Scattering of Light by Small Particles* (John Wiley & Sons, New York, 2008).
[29] L. D. Landau, J. Bell, M. Kearsley, L. Pitaevskii, E. Lifshitz, and J. Sykes, *Electrodynamics of Continuous Media*, Course of Theoretical Physics Series Vol. 8 (Pergamon Press, Oxford, New York, 2013).
[30] B. T. Draine, Astrophys. J. **333**, 848 (1988).
[31] A. B. Evlyukhin, C. Reinhardt, A. Seidel, B. S. Luk'yanchuk, and B. N. Chichkov, Phys. Rev. B **82**, 045404 (2010).
[32] A. D. Humphrey and W. L. Barnes, Phys. Rev. B **90**, 075404 (2014).
[33] G. Schatz, J. Mol. Struct. **573**, 73 (2001).
[34] L. Zhao, K. L. Kelly, and G. C. Schatz, J. Phys. Chem. B **107**, 7343 (2003).
[35] B. Auguié and W. L. Barnes, Phys. Rev. Lett. **101**, 143902 (2008).
[36] S. Rodriguez, M. Schaafsma, A. Berrier, and J. G. Rivas, Physica B **407**, 4081 (2012).
[37] P. A. Belov and C. R. Simovski, Phys. Rev. E **72**, 026615 (2005).
[38] F. J. García De Abajo, Rev. Mod. Phys. **79**, 1267 (2007).
[39] David Yuk Kei Ko and J. C. Inkson, Phys. Rev. B **38**, 9945 (1988).
[40] S. V. Lobanov, T. Weiss, D. Dregely, H. Giessen, N. A. Gippius, and S. G. Tikhodeev, Phys. Rev. B **85**, 155137 (2012).
[41] H. Taniyama and M. Notomi, J. Appl. Phys. **103**, 083115 (2008).

[42] P. Lalanne, W. Yan, K. Vynck, C. Sauvan, and J.-P. Hugonin, Laser Photonics Rev. **12**, 1700113 (2018).
[43] F. De Angelis, G. Das, P. Candeloro, M. Patrini, M. Galli, A. Bek, M. Lazzarino, I. Maksymov, C. Liberale, L. C. Andreani, and E. Di Fabrizio, Nat. Nanotechnol. **5**, 67 (2009).
[44] K. Lodewijks, W. Van Roy, G. Borghs, L. Lagae, and P. Van Dorpe, Nano Lett. **12**, 1655 (2012).
[45] S. R. K. Rodriguez, A. Abass, B. Maes, O. T. A. Janssen, G. Vecchi, and J. Gomez Rivas, Phys. Rev. X **1**, 021019 (2011).
[46] Y. Shen, J. Zhou, T. Liu, Y. Tao, R. Jiang, M. Liu, G. Xiao, J. Zhu, Z.-K. Zhou, X. Wang, C. Jin, and J. Wang, Nat. Commun. **4**, 2381 (2013).
[47] R. Guo, S. Derom, A. I. Väkeväinen, R. J. A. van Dijk-Moes, P. Liljeroth, D. Vanmaekelbergh, and P. Törmä, Opt. Express **23**, 28206 (2015).
[48] G. Vecchi, V. Giannini, and J. Gomez Rivas, Phys. Rev. Lett. **102**, 146807 (2009).
[49] A. Yang, A. J. Hryn, M. R. Bourgeois, W.-K. Lee, J. Hu, G. C. Schatz, and T. W. Odom, Proc. Natl. Acad. Sci. USA **113**, 14201 (2016).
[50] W. Zhou, M. Dridi, J. Y. Suh, C. H. Kim, D. T. Co, M. R. Wasielewski, G. C. Schatz, T. W. Odom *et al.*, Nat. Nanotechnol. **8**, 506 (2013).
[51] D. Wang, A. Yang, W. Wang, Y. Hua, R. D. Schaller, G. C. Schatz, and T. W. Odom, Nat. Nanotechnol. **12**, 889 (2017).
[52] A. Vakevainen, R. Moerland, H. Rekola, A.-P. Eskelinen, J.-P. Martikainen, D.-H. Kim, and P. Torma, Nano Lett. **14**, 1721 (2013).
[53] F. Todisco, M. Esposito, S. Panaro, M. De Giorgi, L. Dominici, D. Ballarini, A. I. Fernández-Domínguez, V. Tasco, M. Cuscuna, A. Passaseo *et al.*, ACS Nano **10**, 11360 (2016).
[54] B. B. Rajeeva, L. Lin, and Y. Zheng, Nano Res. **11**, 4423 (2018).
[55] V. Kravets, A. Kabashin, W. Barnes, and A. Grigorenko, Chem. Rev. **118**, 5912 (2018).
[56] W. Wang, M. Ramezani, A. I. Väkeväinen, P. Törmä, J. G. Rivas, and T. W. Odom, Mater. Today **21**, 303 (2017).
[57] A. Taflove and S. C. Hagness, *Computational Electrodynamics: the Finite-Difference Time-Domain Method* (Artech House, Boston, London, 2005).
[58] P. B. Johnson and R. W. Christy, Phys. Rev. B **6**, 4370 (1972).
[59] D. Maystre, in *Plasmonics* (Springer, Berlin, Heidelberg, 2012), pp. 39–83.
[60] R. Guo, T. K. Hakala, and P. Törmä, Phys. Rev. B **95**, 155423 (2017).
[61] Y. Chu, E. Schonbrun, T. Yang, and K. B. Crozier, Appl. Phys. Lett. **93**, 181108 (2008).
[62] V. G. Kravets, F. Schedin, and A. N. Grigorenko, Phys. Rev. Lett. **101**, 087403 (2008).
[63] See Supplemental Material at http://link.aps.org/supplemental/10.1103/PhysRevB.99.075310 for the reflection, transmission, absorption, and diffraction spectra.
[64] F. B. Craig, F. Bohren, and D. Huffman, Absorption and Scattering of Light by Small Particles (Wiley, New York, 1983).
[65] Q. Bai, M. Perrin, C. Sauvan, J.-P. Hugonin, and P. Lalanne, Opt. Express **21**, 27371 (2013).
[66] P. Y. Chen, D. J. Bergman, and Y. Sivan, arXiv:1705.01747.
[67] P. P. Ewald, Ann. Phys. **369**, 253 (1921).
[68] I. Stevanovic, P. Crespo-Valero, K. Blagovic, F. Bongard, and J. R. Mosig, IEEE Trans. Microwave Theory Tech. **54**, 3688 (2006).
[69] V. G. Papanicolaou, J. Comp. Anal. Appl. **1**, 105 (1999).
[70] F. De Wette and G. Schacher, Phys. Rev. **137**, A78 (1965).
[71] R. E. Collin, *Field Theory of Guided Waves* (McGraw-Hill, New York, 1960).
[72] L. Novotny and B. Hecht, *Principles of Nano-Optics* (Cambridge University Press, New York, 2012).